APL Photonics

Quasi-phase matching waveguides on lithium niobate and KTP for nonlinear frequency conversion: A comparison

Cite as: APL Photonics **6**, 091102 (2021); https://doi.org/10.1063/5.0060096
Submitted: 15 June 2021 • Accepted: 17 August 2021 • Published Online: 08 September 2021

Cristine Calil Kores, Carlota Canalias and Fredrik Laurell

Quasi-phase matching waveguides on lithium niobate and KTP for nonlinear frequency conversion: A comparison

Cite as: APL Photon. 6, 091102 (2021); doi: 10.1063/5.0060096
Submitted: 15 June 2021 • Accepted: 17 August 2021 •
Published Online: 8 September 2021

Cristine Calil Kores, Carlota Canalias, and Fredrik Laurell[a)]

AFFILIATIONS

Department of Applied Physics, Royal Institute of Technology (KTH), Roslagstullsbacken 21, Stockholm 10691, Sweden

[a)]Author to whom correspondence should be addressed: fl@laserphysics.kth.se

ABSTRACT

Established waveguide fabrication technologies on lithium niobate (LN) and potassium titanyl phosphate (KTP) were revisited, and a comparative analysis of their performance for type-0 quasi-phase matched second-harmonic generation at 1.55 μm was provided based on literature data and our simulations. This analysis aided identifying gaps where the waveguide performance is below the theoretical predictions, and the possible reasons are discussed. It provides the reader with a roadmap for choosing the most appropriate waveguide type and material choice between LN and KTP for desired performance of targeted applications.

I. INTRODUCTION

Nonlinear optics (NLO) is an ever-growing field of research enabled by lasers.[1] Because strong light intensities are required for NLO effects to become relevant, such effects can be greatly enhanced when used in waveguides in which light is tightly confined. Only non-centrosymmetric materials, such as the ferroelectric crystals lithium niobate (LN), lithium tantalate (LT), and potassium titanyl phosphate ($KTiOPO_4$, KTP), naturally exhibit a non-zero second-order nonlinearity, $\chi^{(2)}$, which enables wave-mixing processes such as second-harmonic generation (SHG), sum- and difference-frequency generation, and optical parametric amplification.

The development of waveguides for efficient nonlinear optical conversion has been a topic of interest since the 1970s. Early work was devoted to basic studies, primarily based on birefringent phase matching in titanium-diffused LN waveguides, where the material dispersion limited the range of wavelengths accessible.[2] Proton-exchanged (PE) waveguides where developed in the early 1980s, first by Jackel *et al.*,[3] but as they guide only one polarization, they could only be used for nonlinear Cerenkov radiation.[4] The introduction of quasi-phase matching (QPM) waveguides in the late 1980s made the field highly active.[5,6] Conceptually, QPM consists in periodically resetting the phase mismatch between the interacting waves in order to force them to be in phase as they propagate along the nonlinear crystal. As the phase of the generated wave is related to the sign of the $\chi^{(2)}$ nonlinearity, this can be achieved by periodically modulating the crystal structure. It is most commonly carried out by electric field poling, where periodic finger electrodes are placed on the polar face of the ferroelectric crystal, and by applying an electric field, exceeding the crystal's coercive field, over the crystal. Domains of reversed polarization are then created under the electrode fingers. The period, Λ, of the lithographically defined electrode is chosen to compensate for the phase mismatch between the interacting waves, which by design gives flexibility in the choice of interacting wavelengths within the crystal's full transparency range. Furthermore, with QPM, the strongest nonlinearity (d_{33} coefficient) for LN and KTP can be determined, which is inaccessible with birefringent phase matching. An efficient QPM waveguide made by electric field poling was fabricated for the first time in 1993, in LN, by Yamada *et al.*[7] This achievement was a milestone in the field of nonlinear optics, which enabled an improvement of orders of magnitude in NLO conversion. Much of the efforts in the early days were directed toward developing visible sources as compact solid-state lasers were not available in this wavelength range at the time and several applications such as Blu-ray storage and biomedical detection had emerged.[8]

Many such devices have since then been commercialized. The field has attracted renewed attention over the last two decades primarily for its potential application in quantum technologies. In particular, LN waveguide devices have become popular as the key integrated platform for fundamental investigation of quantum phenomena and a variety of paradigm-shifting quantum technologies, such as photon-pair sources, heralded-single-photon sources, coherent frequency-conversion interfaces, and quantum memories.[9–11] In addition, thin-film lithium niobate on insulator (LNOI) has more recently emerged as a hybrid material platform and become commercially available. The thickness of the thin films is usually between 300 and 700 nm,[12] leading to waveguides with submicrometer cross sections, in which the light confinement is dramatically enhanced, enabling extremely efficient NLO conversion. However, the often large propagation and coupling losses exhibited by waveguides on LNOI[13] have so far limited their widespread application, particularly in quantum optical technologies where losses are detrimental.[14]

There are, nevertheless, limitations associated with LN, in particular for operation at visible wavelengths, as the crystal is susceptible to photorefraction,[15] as well as green-induced infrared absorption.[16] In LN, the induced absorption was suggested[16] to be related to the formation of polarons, which consist of electrons trapped by niobium antisite defects. This effect can be reduced by incorporating magnesium oxide, thereby reducing these antisite defects in LN. Alternatively, using stoichiometric LN (when the composition ratio [Li]/([Li]+[Nb]) is 50%) can also reduce the induced absorption. Furthermore, it is also challenging to fabricate the short-period QPM gratings required at these wavelengths. In the visible region, particularly toward shorter wavelengths, KTP is a more suitable material. It exhibits a high optical nonlinearity, excellent mechanical and thermal properties, and high resistance to photorefractive damage,[17,18] as well as to green- or blue-induced infrared absorption especially in the continuous-wave regime. Furthermore, ion-exchanged waveguides in KTP allow a better transverse mode overlap between interacting waves[19] and a better coupling to optical fibers than LN. However, KTP suffers from material homogeneities and a large ionic conductivity, which can affect the quality of the QPM grating negatively and result in inhomogeneous waveguide structures, as well as difficulties with the reproducibility of fabrication.[20] Alternatively, the isomorph rubidium-doped potassium titanyl phosphate (RKTP) can be employed, in which the KTP crystal is doped with typically 0.3% Rb during growth. RKTP exhibits very similar linear and nonlinear optical properties to KTP but has the ionic conductivity reduced by approximately two orders of magnitude,[21] which enhances the quality of both the fabricated QPM structures and the waveguides. In addition, crystals from the KTP family, such as RKTP, offer the possibility of being periodically poled with short periods, which is required for optical interactions at visible wavelengths. Furthermore, if the period is made in the sub-micrometer range, counter-propagating parametric interactions can be analyzed,[22] in which a pump photon generates a forward-propagating signal photon and a narrow bandwidth backward-propagating idler photon. This process is highly interesting, for instance, for the generation of counter-propagating entangled photon pairs.[23] Moreover, KTP and RKTP offer the possibility of group-velocity matching,[24,25] enabling a separable joint-spectral-amplitude diagram, with applications in quantum information technology.[23,26]

For achieving an efficient nonlinear optical conversion, the waveguide should exhibit large nonlinearity, low propagation losses, uniform domain grating and geometry, strong optical confinement, and good mode overlap between the wavelengths involved in the process. Much effort has been dedicated toward the development of waveguides with the above-mentioned requisites fulfilled. This challenging task remains an open topic of research, in which devices are being continually improved.

In this Tutorial, we provide a comparative analysis of different waveguide technologies established for LN and KTP based on literature data and our simulations. The description in Sec. II briefly summarizes the different waveguide technologies, highlighting their most relevant aspects such as refractive index increase, propagation losses, susceptibility to photorefractive damage, and experimental values of conversion efficiency for SHG with the fundamental wavelength at 1.55 μm. For a more extensive description, we refer to the readers elsewhere.[27–31] Simulations of mode profiles were performed in order to calculate the theoretical values of conversion efficiency and coupling efficiency (CE) to single-mode (SM) optical fibers, and the results are presented in Sec. III. Finally, in Sec. IV, results from the literature and simulations identify gaps where the waveguide performance is below the theoretical predictions, and possible improvements are discussed. It provides a roadmap for choosing the most appropriate waveguide type and material choice between LN and KTP to optimize the performance of targeted applications.

II. A COMPARISON BETWEEN DIFFERENT WAVEGUIDE TECHNOLOGIES

An overview of various waveguide technologies on LN, KTP, and RKTP is presented in this section. Their performance is discussed for SHG with the fundamental wavelength at 1.55 μm, unless explicitly stated otherwise. Emphasis is given to technologies based on ion-exchange[32] due to its widespread use; however, other techniques have been successfully demonstrated in both LN and KTP, such as laser writing,[33–36] ion implantation,[37–40] and liquid-phase epitaxy.[41] The diffusion of dopant ions into the crystal structure modifies the crystal's chemical composition, thereby increasing its refractive index, resulting in a waveguiding layer. The solution to the diffusion equation[32] assumes the form of a Gaussian function or a complementary error function (erfc) depending on whether the film was completely depleted during the diffusion process or not, respectively.[42] In the case of proton exchange in LN, the situation is slightly different as the crystal changes phase at high proton concentrations with different diffusion constants in the different phases, resulting in a step-like index profile,[3] as discussed below.

The conversion efficiency for SHG in waveguides is given by $\eta = P_{2\omega}/P_{\omega}$, where P_{ω} and $P_{2\omega}$ are the powers of the fundamental wave, of frequency ω, and the SH wave, of frequency 2ω, respectively. To compare the SHG performance of different waveguides, the normalized conversion efficiency, $\eta_{\mathrm{norm}} = \eta/\left(P_{\omega}L^2\right)$, is used, with a normalization of the input power to 1 W and a waveguide length L of 1 cm. In the low-conversion regime, it is calculated as[8]

$$\eta_{\mathrm{norm}} = \frac{8\pi^2 d_{\mathrm{eff}}^2}{N_{\omega}^2 N_{2\omega} c_0 \varepsilon_0 \lambda_{\omega}^2 A_{\mathrm{ovl}}}, \tag{1}$$

where N_{ω} and $N_{2\omega}$ are the modal refractive indices at the fundamental and SH wavelengths, respectively, λ_{ω} is the fundamental

wavelength, c_0 is the speed of light in vacuum, ε_0 is the vacuum permittivity, and d_{eff} is the effective second-order nonlinear coefficient. The normalized conversion efficiency η_{norm} is used throughout this Tutorial because it allows the comparison between different waveguide technologies independent of the waveguide's length and input power. The overlap area between the transverse modes at the fundamental and SH wavelengths is given by $A_{\text{ovl}} = (I_{\text{ovl}})^{-2}$, where the overlap integral I_{ovl} is defined as[43,44]

$$I_{\text{ovl}} = \frac{\iint E^*_{2\omega}(x,y)E^2_{\omega}(x,y)dxdy}{\left[\iint E^2_{2\omega}(x,y)dxdy\right]^{\frac{1}{2}} \iint E^2_{\omega}(x,y)dxdy}, \tag{2}$$

where E_ω and $E_{2\omega}$ are the electric fields of the fundamental and SH beams, respectively. The unit of the overlap area calculated using Eq. (2) is μm^2. Moreover, in this Tutorial, only z-cut crystals with type-0 QPM is considered where both pump and SH photons exhibit TM polarization; thus, the large d_{33} coefficients of LN and KTP are used, with d_{33} = 32.4 pm/V[45] and d_{33} = 16.9 pm/V,[46] respectively.

The cross sections of some of the most common waveguide geometries are shown in Fig. 1. The comparison presented in this Tutorial comprises two different waveguide geometries, namely, channel waveguides and ridge waveguides. The latter are attractive for NLO conversion because they enable stronger optical confinement than channel waveguides, thus allowing larger conversion efficiencies. The first ridge waveguide fabricated in LN dates back to 1974,[47] fabricated by ion-etching of a planar waveguide. Since then, various techniques have been successfully employed, such as dry etching,[48–50] wet etching,[51] femtosecond-laser structuring,[52] precise-cutting using a diamond tool,[53] and high-precision diamond-blade dicing.[54] The latter has become a popular method since its first demonstration in 2001.[54] In this technique, a rapidly rotating diamond blade is slowly moved along a crystal with a planar waveguide, creating a groove. Two parallel grooves are fabricated, thereby defining a ridge channel waveguide in between them. This method is fast and does not require the use of clean room facilities, and it can provide very smooth side walls, with hardly any chipping, leading to propagation losses as low as α_{loss} = 0.2 dB/cm[55] in LN.

A. Waveguides on lithium niobate

Several techniques to fabricate waveguides on LN have been developed over the last decades, and the main ones based on ion-exchange are described below. The largest value of η_{norm} for type-0 QPM with the fundamental wavelength at 1.55 μm is indicated in each case.

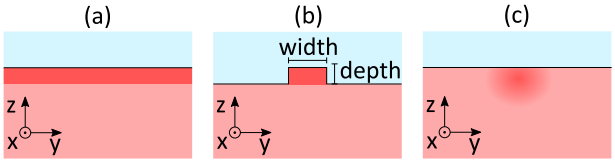

FIG. 1. Illustration of the cross sections of (a) planar, (b) ridge, and (c) indiffused channel waveguides. The width and depth, as used in this Tutorial, are indicated in (b).

1. Ti-indiffused channel waveguides on LN

Waveguide fabrication on LN was first carried out by Ti-indiffusion in the early 1970s,[56,57] and the diffusion dynamics were extensively investigated, resulting in high-quality waveguides for use in electro-optic and nonlinear interactions.[29]

In this technique, a Ti-strip is deposited onto the crystal, followed by heat treatment at temperatures T of ≈ 1100 °C,[58,59] causing diffusion of Ti-ions into the LN crystal, increasing both the extraordinary and ordinary refractive indices, n_e and n_o. If the film is completely depleted during the diffusion process, the resulting refractive index in the z direction assumes a Gaussian profile. The maximum increase at the surface is $\delta n_e(z = 0) \sim 0.022$ and $\delta n_o(z = 0) \sim 0.007$.[56] On z-cut crystals, the diffusion is carried out in the z^--face because in the z^+-face, it can cause spontaneous domain inversion.[58,60,61] Ti-indiffused channel waveguides present low propagation losses of α_{loss} = 0.15 dB/cm,[62] and $\chi^{(2)}$ is fully preserved. However, these waveguides suffer from photorefractive damage (PRD), even at wavelengths as long as 0.85 μm, both for congruent lithium niobate (CLN) and magnesium-oxide doped lithium niobate.[15,63] However, by operating the waveguide at elevated temperatures, 80–120 °C,[64] PRD can be reduced. In the first experimental observation of QPM SHG in an LN waveguide in 1986, periodic Ti-indiffusion enabled a modulation of the linear properties for phase matching, simultaneously creating a domain grating and a waveguide.[65] The best results, however, have been achieved by first creating the Ti-channel waveguide followed by periodically poling the crystal, in which a normalized conversion efficiency of η_{norm} = 21%/(W cm^2) was obtained.[66]

2. Zn-indiffused waveguides

Zn-indiffused waveguides are fabricated in a similar way to the Ti-diffused ones, but it can be performed at slightly lower temperatures, T ≈ 900 °C.[67] When carried out in CLN, it results in an increase in both n_e and n_o, with a Gaussian profile with a maximum index increase at the surface, $\delta n_e(z = 0) = \delta n_o(z = 0) = 0.005$,[68] and propagation losses as low as α_{loss} = 0.3 dB/cm (measured at 633 nm).[69] $\chi^{(2)}$ is largely preserved,[67] and as opposed to Ti-indiffused waveguides, they exhibit very low photorefractive damage.[69] The largest efficiency demonstrated in Zn-indiffused channel waveguides was η_{norm} = 59%/(W cm^2).[67] Diamond-blade diced ridge waveguides have also been demonstrated in Zn-indiffused LN, in which η_{norm} = 9%/(W cm^2) was achieved. The lower efficiency, when compared to purely indiffused channel waveguides, was attributed to larger scattering losses at the sidewalls.[70]

3. Proton-exchanged and annealed proton-exchanged waveguides

Proton exchange[71] is an ion-exchange technique in which the crystal is immersed in a liquid source of hydrogen ions; the most commonly used ones are pyrophosphoric acid[72] or benzoic acid.[33] The replacement of lithium ions (Li^+) by hydrogen ions (H^+) leads to a compositional modification referred to as $Li_{1-x}H_xNbO_3$. If the acidity is strong, which is the case when the acids are undiluted, a large amount of H^+ (up to x = 70%) replaces the Li^+-ions, with an additional structural modification from the original crystalline α-phase to a cubic phase with a complete loss of the optical nonlinearity.[73] Up to seven different phases have been identified in

the PE layers,[74] and most of them exhibit high propagation losses and strongly reduced electro-optic and nonlinear coefficients.[75,76] The ion-exchange causes a step-like refractive index profile with an increase in n_e up to $\delta n_e \approx 0.14$ and a corresponding decrease in n_o down to $\delta n_o \approx -0.06$.[77] This means that the PE layer can guide a single polarization only, i.e., TM modes for z-cut LN. Subsequent to PE, a heat treatment can be used to further diffuse the H^+-ions into the crystal, forming the so-called annealed proton-exchanged (APE) waveguides. The initial step-like refractive index profile then evolves into an exponential profile and, with continued annealing, to a Gaussian profile.[78] Annealing under proper conditions (time and temperature)[78] can fully restore the crystalline structure to the α-phase[74] and thereby regaining the $\chi^{(2)}$ nonlinearity.[72,76,79,80] The propagation losses are then also reduced to $\alpha_{loss} \approx 0.15$ dB/cm[81] (measured at 800 nm), while the surface refractive index increase is reduced to $\delta n_e(z = 0) = 0.02$ with the waveguide depth approximately seven times larger than that just after PE.[78]

APE waveguides present advantages such as a low processing temperature, T ≈ 250–300 °C, and a high resistance to photorefractive damage;[82] however, as the diffusion of protons takes place both sidewise and in depth, it gives an asymmetric refractive index profile and elliptical modes, resulting in poor overlap between the fundamental (TM_{00}) modes at the fundamental and SH wavelengths. Variants in PE have been successfully demonstrated, such as soft proton exchange (SPE),[83] high-index soft proton-exchange,[84] vapor-phase proton-exchange,[85] and high-vacuum vapor-phase proton-exchange.[86] These techniques are attractive because they maintain $\chi^{(2)}$ without being affected; however, very accurate control of the fabrication conditions is required to obtain reproducible results.

The largest normalized conversion efficiency demonstrated with APE channel waveguides was $\eta_{norm} = 65\%/(W\ cm^2)$,[87] while for SPE channel waveguides, $\eta_{norm} = 48\%/(W\ cm^2)$ has been obtained.[88]

APE ridge waveguides have been successfully fabricated by dicing with propagation losses as low as 0.1 dB/cm.[89] The largest conversion efficiency demonstrated for such APE ridge waveguides was $\eta_{norm} = 80\%/(W\ cm^2)$, achieved in commercial samples from HC Photonics.[90]

4. Reverse proton-exchanged waveguides

If APE waveguides are processed in a lithium-rich melt, Li^+-ions will diffuse into the surface layer, while H^+-ions will diffuse out. This results in a more symmetric refractive index profile and, consequently, a much improved overlap between the modes of the fundamental and the SH waves. The waveguides resulting from this process are referred to as reverse proton-exchanged (RPE) waveguides. Similar to APE waveguides, they guide only one polarization, they present low propagation losses, as low as $\alpha_{loss} = 0.1$ dB/cm,[91,92] and $\chi^{(2)}$ is partially or fully restored.[72,79,80] The largest normalized conversion efficiency demonstrated in RPE channel waveguides was $\eta_{norm} = 150\%/(W\ cm^2)$.[93]

5. Thin-film waveguides

Thin-film waveguides exhibit a large refractive index contrast between the film and the substrate and symmetric optical-mode profiles with maintained material properties. Altogether, this leads to a very small modal cross section with a good overlap between the interacting modes, allowing for efficient nonlinear interaction at low input power. There are two main techniques employed for the fabrication of LN thin-film waveguides. The first technique is based on crystal ion slicing, which was developed in the late 1990s,[94] resulting in the so-called lithium niobate on insulator (LNOI), in which submicrometer film thicknesses can be achieved with high homogeneity. In the second technique, LN is first bonded to a substrate using either an adhesive[54] or by direct bonding;[95] thereafter, the LN crystal is polished until the desired thickness is achieved,[96] resulting in the so-called adhered waveguides. This method enables the realization of films with thicknesses as low as a few micrometers.

The commercial availability of LNOI has boosted the development of new devices over recent years. As the waveguide dimensions decrease, the impact of waveguide imperfections on the optical modes increases, and consequently, fabrication tolerances become very strict. In particular, propagation losses are typically large due to a large electric field strength at the waveguide sidewalls and scattering due to sidewall roughness. This becomes detrimental as the mode size is reduced here. There have recently been considerable efforts to reduce the sidewall roughness,[97–99] leading to propagation losses as low as $\alpha_{loss} = 0.027$ dB/cm using dry etching[100] and to $\alpha_{loss} = 0.03$ dB/cm using chemo-mechanical polishing.[101,102] A major remaining challenge is the coupling of light in and out of LNOI waveguides as the dimensions are very small. The mode-mismatch for conventional optical fiber end-face coupling leads to coupling efficiencies of only CE ≈ 3%. Alternative more complex coupling schemes have been successfully implemented, such as use of grating couplers (CE ≈ 45%[103]), a tapered fiber (CE ≈ 65%[104]), and an inverse waveguide taper combined with a tapered fiber (CE ≈ 68%[105]).

The first demonstration of outstanding QPM SHG performance in an LNOI waveguide was carried out in 2018 by Wang *et al.*, when a normalized conversion efficiency, $\eta_{norm} = 2600\%/(W\ cm^2)$, was achieved.[106] In the following year, a waveguide was made where the QPM structure was optimized by monitoring the SH response during periodic poling, with $\eta_{norm} = 4600\%/(W\ cm^2)$, which is the largest reported η_{norm} for LN to date.[107]

The technique to fabricate adhered thin films requires extremely accurate control of the polishing step in order to produce homogeneous waveguides. The highest efficiency $\eta_{norm} = 370\%/(W\ cm^2)$ in this case was demonstrated with a multimode adhered ridge waveguide fabricated on a 5 mol. % Zn-doped LN substrate.[108]

B. Waveguides on KTP

In this section, waveguide technologies based on ion-exchange in KTP and RKTP are described. The ion diffusion in KTP is highly anisotropic, with the diffusion coefficient several orders of magnitude larger in the z direction than in the x and y directions[20] due to the open chiral channels present in the z direction of the crystal.[21] There has been significantly less research studying waveguides in KTP than in LN. Much of the efforts in the late 1980s and 1990s were toward developing blue-light sources via nonlinear processes[109,110,122] since KTP is less susceptible to photochromic damage than LN. Therefore, in this section, SHG at the blue wavelength region is sometimes mentioned rather than at 1.55 μm, for means of comparing the performance of different waveguides.

1. Ion-exchange in KTP and RKTP

Ion-exchange can be carried out in KTP or in RKTP to fabricate waveguides, with univalent ions such as Cs^+, Tl^+, or Rb^+ as

dopants.[19] As the K^+-ions close to the surface diffuse out of the crystal, they leave K-vacancies behind. These are negatively charged and electrostatically attract dopant ions in the melt, which enter the crystal to counteract the charge unbalance. The vacancies are highly mobile and can act as hopping centers for the ions. Moreover, pre-existing vacancies also attract dopant ions from the melt.[111] $RbNO_3$ melts are the most commonly used exchange baths, and the resulting compositional modification is referred to as $Rb_xK_{1-x}TiOPO_4$.

The ionic conductivity in flux-grown KTP is often inhomogeneous over the grown boule and hence also in the wafer cut for waveguide fabrication. It can vary by as much as one order of magnitude along the *y* direction[21] due to a spatial variation in vacancies, while it is more or less constant in the x-direction.[112] Consequently, the depth of Rb-exchanged waveguides varies particularly for those with propagation in the y direction.[58] This has hampered commercial production of KTP waveguides. RKTP is an interesting alternative to KTP for waveguide fabrication. It shows a much lower ionic conductivity than KTP as a result of the larger ionic radius of Rb^+ than that of K^+, which reduces the diffusivity in the ionic channels in the crystal network. As the Rb-exchange progresses and the concentration of Rb in the surface layer increases, the crystal's conduction channels[21] become more and more blocked, suppressing further ion-exchange and reducing the achievable diffusion depth.[19] A consequence of this process is that ion-exchange in KTP or RKTP does not obey simple diffusion kinetics, as already noted in earlier works.[19] Another consequence of the lower ionic conductivity is that the conditions for ion-exchange in RKTP are different than those in KTP. On the other hand, a positive aspect from the larger Rb^+-ions being less mobile in the RKTP lattice than in KTP is that Rb-exchanged waveguides in RKTP are much more stable than those made in KTP, in which the Rb^+-ions diffuse over time when the waveguide is operated at high optical powers,[112] thereby changing their performance.

Divalent ions such as Ba^{2+} or Sr^{2+} can be added to the melt in order to increase the ion-exchange rate. Most commonly, $Ba(NO_3)_2$ is added to the exchange bath, and each Ba^{2+}-ion will diffuse into the crystal together with a vacancy, thereby replacing two monovalent ions (K^+), to provide charge neutrality. The increase in the K-vacancy concentration increases the ionic conductivity and thus the ion-exchange rate for Rb^+.[111] Approximately, a 5% concentration of Ba can be incorporated in the crystal lattice without changing the crystal's structure or its optical properties significantly.[111] However, a larger Rb-concentration enabled by the divalent ions in the melt increases the strain in the crystal, which can lead to spontaneous domain reversal,[113,114] deteriorating the domain grating in PP crystals. The addition of K^+-ions to the melt reduces the maximum Rb-concentration in the crystal, while still maintaining a deep enough diffusion depth.[111] To optimize the ion-exchange process, one should consider the delicate interplay between several parameters, such as surface quality, ionic conductivity, melt composition, and processing temperature.

There are no prior studies that have systematically investigated the ion-exchange dynamics in KTP or RKTP, although recent studies contributed significantly to understanding this complex process.[115,116] The ion diffusion has a complementary error–function profile, which causes both n_e and n_o to increase with the same profile. The maximum increase in the surface refractive index is up to $\delta n_o(z = 0) = \delta n_e(z = 0) = 0.024$ in the *z* direction for KTP.[19] To this date, there are no corresponding available experimental data for the surface refractive index increase in RKTP.

The crystalline structure of KTP, RKTP, and RTP is the same and unaltered by the ion-exchange, which also holds good for $\chi^{(2)}$,nonlinearity, in strong contrast to PE in LN, where the crystal goes through phase transitions and $\chi^{(2)}$ is reduced. However, the temperature change during ion-exchange can result in strong internal fields and lead to spontaneous domain reversal when the domain walls are initially charged,[116] as is the case when the domain walls are tilted (non-parallel to the polar axis). Tilted domains normally appear when the domains have not propagated fully through the crystal and stabilized or when they have broadened during periodic poling.[116]

2. Segmented ion-exchanged waveguides

It has been shown that spontaneous domain reversal can appear during Rb/Ba ion-exchange on the z^--side of KTP. By using a segmented mask for exchange, a waveguide and a QPM structure could simultaneously be obtained.[113,117] Such waveguides show high normalized conversion efficiencies, η_{norm} = 112–250%/(W cm^2) for type-0 QPM SHG at blue wavelengths, 425 nm.[27,117] More than 40% of the light incident on these segmented waveguides is transmitted, indicating that the propagation losses are low.[27]

3. Ion-exchanged channel waveguides

For regular, straight channel waveguides fabricated in periodically poled KTP, a normalized conversion efficiency of η_{norm} = 2%/(W cm^2) has been reported for type-0 QPM SHG at 400 nm.[118] The propagation losses in these waveguides were α_{TM} = 1.3 dB/cm and α_{TE} = 1.8 dB/cm for TM and TE polarizations, respectively, measured at 890 nm. In periodically poled RKTP channel waveguides, η_{norm} = 115%/(W cm^2) was demonstrated for type-0 QPM SHG at 470 nm.[116] The larger value is attributed to a more homogeneous waveguide on RKTP than on KTP.

4. Ion-exchanged ridge waveguides

Diamond-blade diced ridge waveguides have been successfully fabricated in both KTP and RKTP. In Rb-exchanged KTP, type-II QPM SHG at 396 nm was reported with η_{norm} = 6.6%/(W cm^2),[119] in which an upper limit for the propagation losses was estimated as α_{loss} = 6 dB/cm. Waveguides with lower loss have been demonstrated in Rb-exchanged ridge waveguides in KTP, with measured loss values at 1.55 μm of α_{TE} = 1.3 dB/cm and α_{TM} = 1.6 dB/cm for TE and TM polarizations, respectively.[120]

In KTP waveguides fabricated by carbon-ion implantation followed by dicing, birefringent phase matching for SHG with a fundamental wavelength of ≈ 1 μm resulted in η_{norm} = 1.12%/(W cm^2) in samples with losses of α_{loss} = 1.5 dB/cm.[121]

Type-0 SHG with a fundamental wavelength of 934 nm has also been reported in RKTP,[122] with η_{norm} = 31%/(W cm^2) as an upper limit. Since the fabricated waveguides showed non-negligible scattering losses, the fundamental power at the output of the waveguide was used for the calculation of η_{norm}; therefore, this result corresponds to an upper limit.

5. Thin films

Adhered ridge waveguides in KTP have been successfully fabricated by bonding and polishing to fabricate the thin films and

diamond-blade dicing for fabricating the ridge waveguides.[123] They were investigated for birefringent type-II SHG phase matching with the pump wavelength at 1.12 μm, and a conversion efficiency of 3.4% was achieved. The waveguide propagation losses were estimated to be α_{TM} = 0.6 dB/cm and α_{TE} = 1.6 dB/cm.

III. SIMULATIONS

Most of the waveguide types presented in Sec. II have been modeled with the goal of simulating their performance for type-0 QPM SHG at 1.55 μm. The simulation constraints are presented in Sec. III A, and the simulation results are presented in Sec. III B.

A. Simulations constraints and parameters

Ion-exchanged waveguides on LN and KTP as well as ridge waveguides on LNOI have been simulated using the finite element analysis platform COMSOL, in which the geometry of each waveguide is given as an input to the software. The details for each case are described in the corresponding sections. The software then solves the frequency domain form of Maxwell's equations using the finite element method. The resulting electric field transverse distribution is then the figure of interest. The calculations were performed for first order (m = 1), type-0 QPM with TM polarization on z-cut CLN and KTP, thus using the strongest nonlinear coefficient, d_{33}. Furthermore, only single-mode waveguides at 1.55 μm were considered. The waveguides' lateral and vertical directions are y and z, respectively, and light propagates along the x-direction. Given these considerations, the waveguides' cross sections were modeled, and the resulting transverse mode profiles TM_{00} at the fundamental and SH wavelengths of 1.55 μm and 775 nm, respectively, were used to calculate the overlap area A_{ovl} using Eq. (2), with the integral limits extended to infinity. The effective refractive indices of the fundamental and SH waveguide modes, N_ω and $N_{2\omega}$, respectively, as well as A_{ovl} were then used to calculate η_{norm} using Eq. (1). In addition, the coupling efficiency between the waveguide's TM_{00} mode at 1.55 μm and a standard single-mode optical fiber SMF28 was calculated via the overlap integral, with the fiber end coupled to the waveguide.

In all the simulations presented here, the extraordinary refractive index, n_e, was considered to linearly depend on the ion-concentration profile C(y, z). Furthermore, the extraordinary refractive index increase on the surface, δn_e(z = 0), always assumed the maximum values reported in the literature to provide maximum confinement (see Sec. II).

The simulations were performed by varying the waveguide width w and depth d in the entire range where the waveguide was single mode at 1.55 μm, while considering the maximum refractive index increase resulting from each waveguide fabrication method. A summary of the refractive index profiles and values of δn_e(z = 0) used in the simulations is shown in Table I.

TABLE I. Summary of the simulation parameters.

Waveguide type	Profile of n_e(z)	Profile of n_e(y)	δn_e(z = 0)
Ti-indiffused LN, channel	Gaussian	erfc	0.022
Zn-indiffused LN, channel	Gaussian	erfc	0.005
APE LN, channel	Gaussian	erfc	0.02
RPE LN, channel	Gaussian[a]	erfc	0.02[a]
APE LN, ridge	Gaussian	Uniform	0.02
LNOI, ridge	Uniform	Uniform	0.75[b]
Rb-indiffused KTP, channel	erfc	Uniform	0.02
Rb-indiffused KTP, ridge	erfc	Uniform	0.02

[a]A symmetric Gaussian profile, with the maximum buried rather than on the surface.
[b]Considering the refractive index contrast between LN and the substrate, SiO_2.

B. Simulation results

The simulation results of channel waveguides in LN are shown in Fig. 2, of LN ridge waveguides are shown in Fig. 3, and of channel and ridge waveguides in KTP are shown in Fig. 4. Each figure contains the calculated values of the overlap area A_{ovl}, normalized conversion efficiency η_{norm}, and coupling efficiency to an SM optical fiber. The results are expressed in terms of the waveguide's width w and depth d, which result from the ion-exchange process.

The results in Figs. 2(a1)–2(d1) and 4(a1) illustrate that under certain conditions for the waveguide geometry, A_{ovl} decreases as the waveguide width increases. This counter-intuitive behavior is present for all the channel waveguides based on ion diffusion. This effect is due to the weak mode confinement of narrow waveguides such that as their dimensions increases, they get a stronger mode confinement, thereby decreasing the overlap area. This effect is not present in any of the ridge waveguides, given that the refractive index contrast with air is always large. Nevertheless, for LNOI ridge waveguides, A_{ovl} is larger for small depths, i.e., film thickness, due to the weaker mode confinement as the dimensions approach the lower limit for confining the mode.

From Eq. (1), it is evident that η_{norm} increases with decreasing A_{ovl}. The values of A_{ovl} achieved with each waveguide technology, as shown in Figs. 2(a1)–2(d1), 3(a1)–3(d1), and 4(a1)–4(d1), are a result of how strong the mode confinement is and of how good the overlap between the transverse-mode profiles at the fundamental and SH wavelengths is. When comparing the values of A_{ovl} obtained with channel waveguides with the values obtained with ridge waveguides, the advantage becomes evident for the latter in terms of mode confinement. The sub-micrometer width of LNOI ridge waveguides leads to extremely small values of A_{ovl} and thus extremely large values of η_{norm}, as shown in Fig. 3(b). Moreover, the values of A_{ovl} obtained with RPE channel waveguides are evidence of the improved mode overlap achieved in this type of waveguide.

It is noteworthy that the coupling efficiency (CE value), shown in Figs. 2(a3)–2(d3), 3(a3)–3(d3), and 4(a3)–4(d3), is larger for channel waveguides than for ridge waveguides due to a weaker mode confinement. Moreover, waveguides in KTP can have close to circular modes and hence exhibit excellent mode matching to fibers.

IV. COMPARISON AND DISCUSSION

In this final section, a discussion comparing the simulation results and the literature results is presented, highlighting the advantages and limitations of each waveguide technology. In the following, the presented comparison is simplified in the sense that it is assumed that $\chi^{(2)}$ was completely preserved and that propagation losses were negligible. However, these two assumptions are not always appropriate, as discussed in detail in the individual descriptions of each

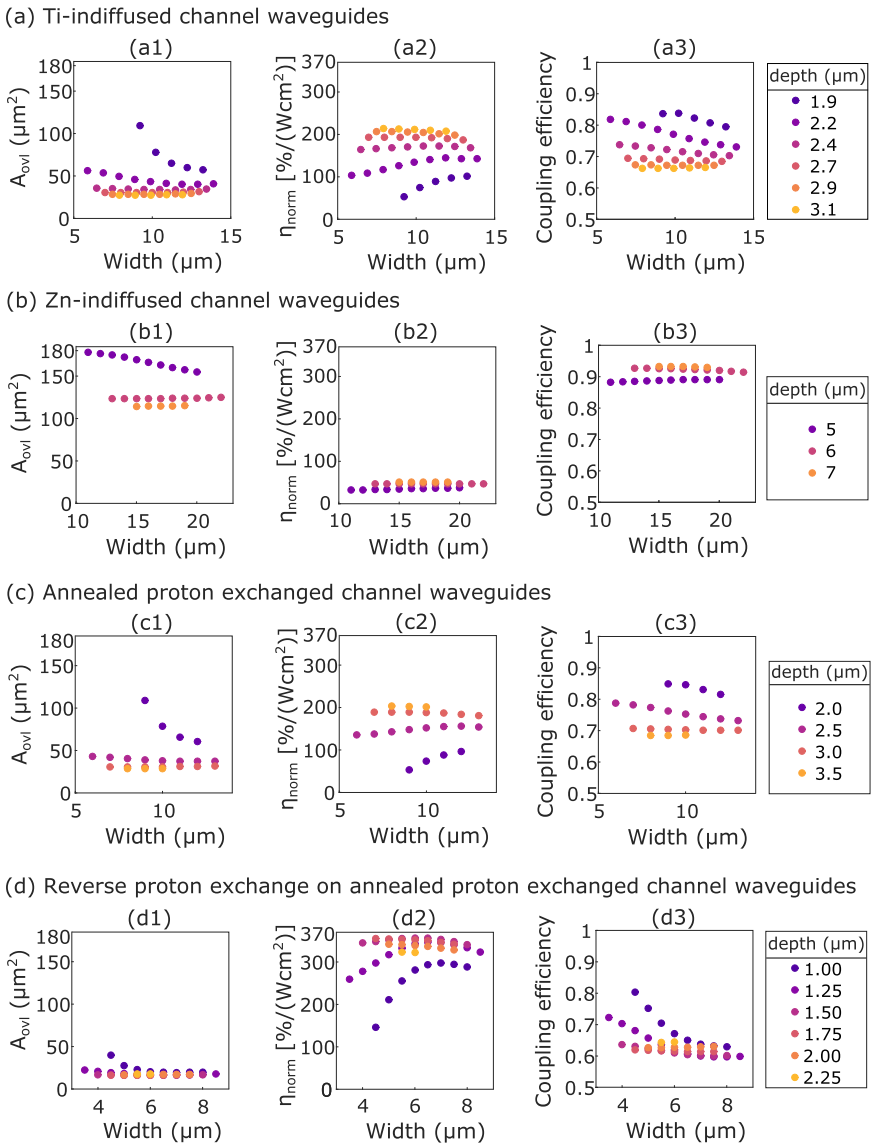

FIG. 2. Calculations for channel waveguides in LN of the overlap area between TM_{00} modes at the fundamental and second-harmonic wavelengths (a1)–(d1), normalized conversion efficiency (a2)–(d2), and coupling efficiency between the TM_{00} mode at the fundamental wavelength and a single-mode optical fiber (a3)–(d3).

waveguide type in Secs. II A and II B. In the simulations, it was also assumed that the evanescent field of the guided modes (at the fundamental and SH waves) outside the waveguide region is negligible. This assumption enables the calculation of I_{ovl} with the integration limits in Eq. (2) extend to infinity. This assumption is a good approximation for the ion-exchanged waveguides considered in the simulations; however, it is less appropriate for LNOI waveguides. In an LNOI waveguide, the optical fields become less confined to the guiding region as the waveguide dimensions are decreased, leading to an overestimation of the calculated η_{norm}.[107]

Figure 5(a) displays the efficiency values extracted from Figs. 2(a3)–2(d3), 3(a3)–3(d3), and 4(a3)–4(d3). The lower bound of each range can, of course, be decreased by reducing $\delta n_e(z = 0)$ used in the simulations. The calculated values of η_{norm} achieved with the different types of waveguides are shown as a solid fill, and the tremendous enhancement achievable with LNOI waveguides is clear in Fig. 5(a). The values of η_{norm} multiplied by the coupling efficiencies between the TM_{00} mode at 1.55 μm and a single-mode optical fiber are also displayed in Fig. 5 (patterned fill). This multiplication is not carried out for LNOI ridge waveguides, for which end-fire coupling with a fiber is too inefficient. For SHG, this product corresponds to an input coupling efficiency, with a fundamental wavelength of 1.55 μm. The overall efficiency of the device consists of a multiplication of the input coupling efficiency, η_{norm}, and the output coupling efficiency, i.e., the collection efficiency of a single-mode fiber.

In many applications, a low value of η_{norm} can be compensated for by increasing the power of the fundamental field. For spontaneous parametric down-conversion (SPDC) with generated photons at 1.55 μm, the multiplication displayed in Fig. 5 corresponds to

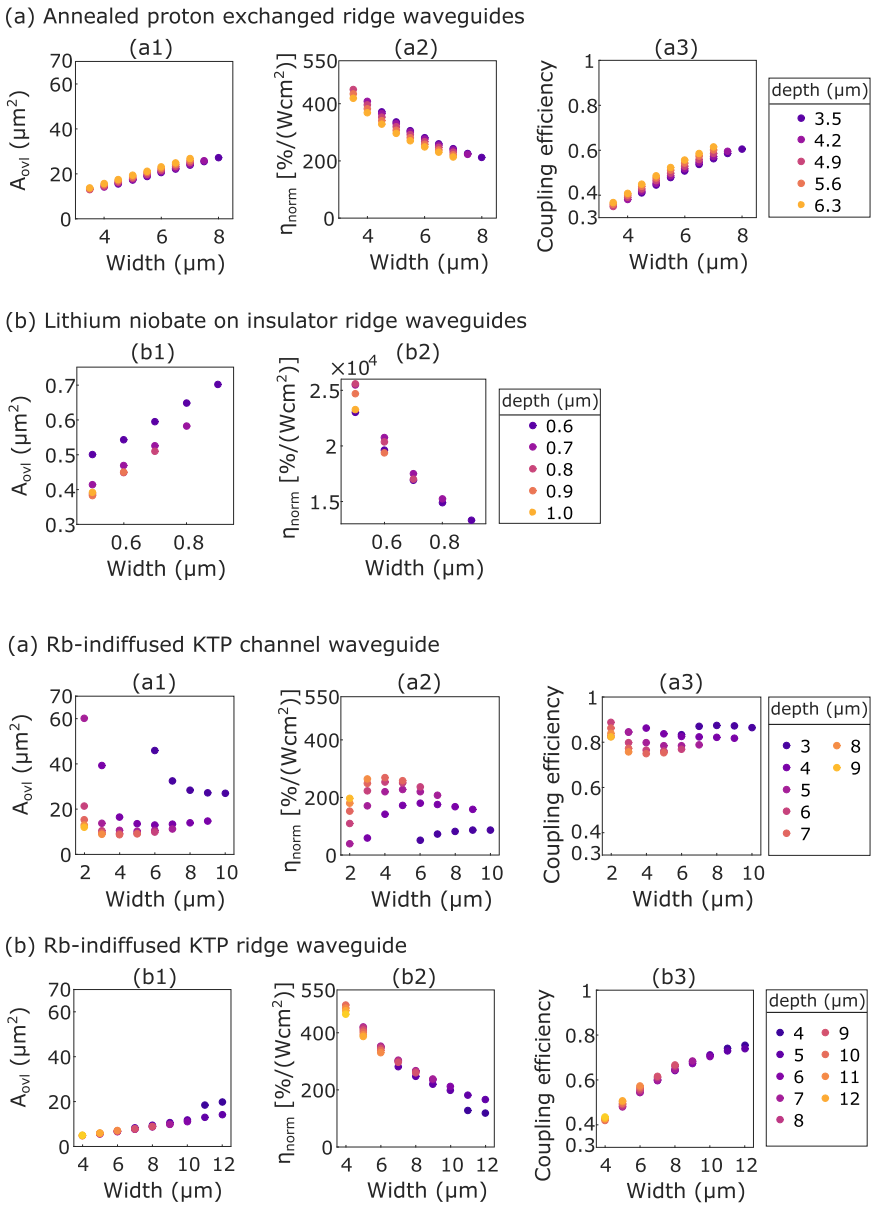

FIG. 3. Calculation for ridge waveguides on LN of the overlap area between TM_{00} modes at the fundamental and second-harmonic wavelengths (a1) and (b1), normalized conversion efficiency (a2) and (b2), and coupling efficiency between the TM_{00} mode at the fundamental wavelength and a single-mode optical fiber (a3) and (b3) calculated for (a), while for (b), this is not an appropriate coupling method.

FIG. 4. Calculation of the overlap area between TM_{00} modes at the fundamental and second-harmonic wavelengths (a1) and (b1), normalized conversion efficiency (a2) and (b2), and coupling efficiency between the TM_{00} mode at the fundamental wavelength and a single-mode optical fiber (a3) and (b3). The calculations concern different waveguides in KTP.

an output coupling efficiency, when a single-mode optical fiber is used to collect the generated photons. For applications in quantum information technology, for instance, when the device is an entangled-photon-pair source based on SPDC, then η_{norm} and the coupling efficiency should be considered separately. In this case, the output coupling efficiency is a severe limiting factor for the technological application, often preventing these devices from reaching the efficiency levels achieved with bulk optics.[11]

The record experimental values of η_{norm} reported in the literature are included in Fig. 5(b) for waveguides on LN at 1.55 μm. To our knowledge, waveguides on KTP have not been used for SHG with a fundamental wavelength at 1.55 μm. Overall, the results indicate that the device performances generally remain below the theoretical values, with the exception of Zn-indiffused channel waveguides in LN. The maximum calculated value for η_{norm} in Zn-indiffused channel waveguides in LN is slightly below the maximum value demonstrated experimentally. This is most likely due to the fact that in Ref. 67, the fabrication conditions lead to a larger δn_e than what was considered in the simulations. Regarding the LNOI ridge waveguides, the indicated record value was achieved by using a lensed fiber for coupling,[107] leading to CE = 25%.

A summary of relevant parameters for comparing the overall performance of different waveguides is given in Table II. It is noteworthy that the indicated values of CE serve as a comparison between the different technologies as they were calculated considering the maximum $\delta n_e(z = 0)$ resulting from each waveguide

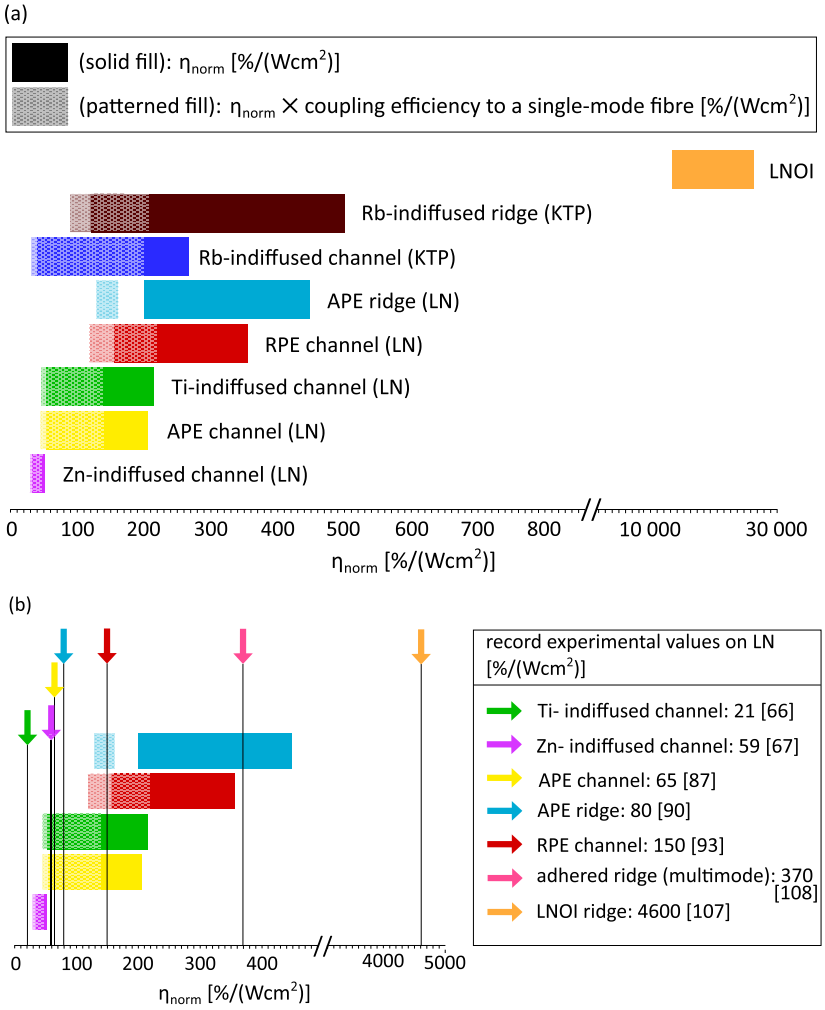

FIG. 5. (a) Normalized conversion efficiency (solid fill) for SHG with a fundamental wavelength of 1.55 μm for different types of single-mode waveguides on lithium niobate and on KTP. The patterned fill corresponds to the calculated normalized conversion efficiency multiplied by the coupling efficiency to a single-mode optical fiber. (b) The record value of the normalized conversion efficiency reported in the literature is additionally displayed for each waveguide type on LN.

fabrication method. In some cases, the CE could be improved by adjusting the waveguide mode area to match the mode area of the optical fiber better. This could be achieved in practice by reducing $\delta n_e(z = 0)$, albeit at the cost of also reducing A_{ovl}. In particular, the largest fiber coupling efficiency reported for RPE/APE channel waveguides was 90%,[91] while our simulations indicate a value of 80%.

The difference between the theoretically calculated efficiencies and the often lower experimental results is due to different technological difficulties, which have not yet been fully solved, such as combining periodic-poling technology with waveguide fabrication technologies, large propagation losses (in the case of ridge wavebreak guides), and inhomogeneity in the waveguide dimensions and/or in the QPM structure. While propagation and coupling losses reduce the overall transmission in the waveguide, thus decreasing the conversion efficiency, the above-mentioned inhomogeneities cause an asymmetry in the phase matching curve and drastically reduce the conversion efficiency.[124]

The results in Fig. 5 and Tables I and II indicate that waveguides on KTP present very promising conversion and coupling efficiencies once the challenges associated with the waveguide fabrication are overcome. It is worth mentioning that the experimental results of conversion efficiency shown for KTP waveguides are for SHG in the blue region as this is the available data in the literature. Nevertheless, at such shorter wavelengths, the values of A_{ovl} are smaller than those in the IR; thus, an even larger theoretical η_{norm} is expected. In particular, the excellent performance of channel waveguides is mainly due to the negligible transverse Rb-diffusion along the y direction, when compared to the diffusion in depth along the z direction. The resulting refractive index profile contributes to a strong mode confinement and means to obtain circular modes, thereby obtaining very high coupling efficiency to optical fibers. The data presented in Fig. 5 show that the calculated performance of channel waveguides in KTP is typically better than that of channel waveguides in LN, with the exception of RPE channel waveguides.

When comparing the simulated values of η_{norm} for ridge waveguides on APE LN and on Rb-exchanged KTP, the values are slightly larger for the latter, even though d_{33} in LN is almost twice as large as d_{33} in KTP.[45,46] However, when comparing the materials, the figure of merit,[1] FOM = $d_{33}/(n_\omega n_{2\omega}^2)$, is only ~15% smaller for KTP than

TABLE II. Parameters for comparing different waveguide technologies on LN and KTP. The normalized conversion efficiency values η_{norm} refer to type-0 QPM, with TM_{00} modes at the fundamental (1.55 μm) and second-harmonic wavelengths, in the CW low-conversion regime. The propagation losses α_{loss} and the coupling efficiency (CE) to an SM optical fiber are given at 1.55 μm.

Waveguide type	Expt. η_{norm} [%/(W cm^2)]	Sim. η_{norm} [%/(W cm^2)]	Expt. α_{loss} (dB/cm)	PRD	Simul. CE	Modes
Ti-indiffused LN, channel	21[66]	215	0.15[62]	Yes	0.84	TE/TM
Zn-indiffused LN, channel	59[67]	51	0.85[67]	No	0.93	TE/TM
APE LN, channel	65[87]	205	0.15[a,81]	Yes[b]	0.85	TM
RPE LN, channel	150[93]	356	0.09[91]	Yes[b]	0.80	TM
APE LN, ridge	80[90]	450	0.1[89]	Yes[b]	0.61	TM
LNOI, ridge	4600[107]	25 500	0.03[100]	Yes[b]	⋯	TE/TM
Rb-indiffused KTP, channel	2[c,118] 115[d,116]	268	1.3[e,118]	No	0.89	TE/TM
Rb-indiffused KTP, ridge	31[f,122]	500	1.6[120]	No	0.75	TE/TM

[a]Measured at 800 nm.
[b]May be reduced by using MgO-doped LN.
[c]SHG at 425 nm.
[d]SHG at 470 nm in RKTP.
[e]Measured at 890 nm.
[f]SHG at 470 nm in RKTP; corresponds to an upper limit (see Ref. 122).

that of LN. This result indicates that $n_e(z)$ according to an error function leads to improved efficiencies when compared to $n_e(z)$ according to a Gaussian function.

Recent progress on LNOI has shown that it is feasible to achieve low propagation losses of α_{loss} = 0.03 dB/cm,[100–102] a large CE value of 68%,[105] and good homogeneity and thus a conversion efficiency as large as 4600%/(W cm^2).[107] These extremely promising results were demonstrated in different devices, and combining the state of the art fabrication processes in a single device would potentially enable LNOI waveguides to replace traditional waveguides on LN. For applications in quantum optics, however, further improvement in the CE value is still paramount, particularly on the collection side, as both photons in entangled pairs are needed for system applications.

V. CONCLUSIONS

The results presented in this Tutorial call attention to the fact that there is a need for further improvement of waveguides used for NLO interactions. Regarding lithium niobate, the SHG performance of Ti-indiffused, APE, and RPE channel waveguides, as well as APE ridge waveguides, remains ~2–10 times below the theoretical values, as shown in Table II. The experimental values of propagation losses are low, indicating that their sub-optimal performance is likely due to a non-ideal mode overlap between fundamental and SH fields and to a partially unsuccessful combination of technologies for domain reversal and ion-exchange. On the other hand, the performance of Zn-indiffused channel waveguides is similar to the theoretical values, indicating that the fabrication process is well optimized, but the maximum theoretical conversion efficiency in these waveguides is limited by the large mode profiles. Regarding waveguides in the KTP family, both Rb-indiffused channel waveguides in KTP and RKTP have been demonstrated with high efficiencies. The latter are also more stable, which is attributed to RKTP's lower ionic conductivity and higher spatial homogeneity, allowing repeatable fabrication of homogeneous waveguides and high-quality domain gratings. Nevertheless, the performance of Rb-indiffused channel waveguides in RKTP is still approximately two times lower than the theoretical value, indicating that the ion-exchange parameters can be further improved.

In addition, the results presented in this Tutorial were constrained to ion-diffused waveguides. Nevertheless, other waveguide fabrication techniques are also highly relevant, such as ion implantation and fs-laser writing. Breakthroughs in these techniques could prove them to be more viable and flexible than the traditional techniques based on ion-exchange.

ACKNOWLEDGMENTS

We acknowledge the financial support from the Swedish Foundation for Strategic Research (SSF Grant No. RMA15-0135), the Knut and Alice Wallenberg Foundation (project "Photonic Quantum Information"), the Olle Engkvist Foundation, and the Swedish Research Council.

DATA AVAILABILITY

All experimental data in this article are taken from the cited references. The simulation results of the overlap area, normalized conversion efficiency, and coupling efficiency are the results of calculations with the given equations.

REFERENCES

[1]P. N. Butcher and D. Cotter, *The Elements of Nonlinear Optics* (Cambridge University Press, 1990).
[2]G. I. Stegeman and C. T. Seaton, J. Appl. Phys. **58**, R57 (1985).
[3]J. L. Jackel, C. E. Rice, and J. J. Veselka, Appl. Phys. Lett. **41**, 607 (1982).
[4]N. A. Sanford and J. M. Connors, J. Appl. Phys. **65**, 1429 (1989).
[5]J. Webjörn, F. Laurell, and G. Arvidsson, J. Lightwave Technol. **7**, 1597 (1989).
[6]E. J. Lim, M. M. Fejer, R. L. Byer, and W. J. Kozlovsky, Electron. Lett. **25**, 731 (1989).

[7]M. Yamada, N. Nada, M. Saitoh, and K. Watanabe, Appl. Phys. Lett. **62**, 435 (1993).
[8]W. P. Risk, T. R. Gosnell, and A. V. Nurmikko, *Compact Blue-Green Lasers* (Cambridge University Press, 2003).
[9]S. Tanzilli, H. De Riedmatten, W. Tittel, H. Zbinden, P. Baldi, M. De Micheli, D. B. Ostrowsky, and N. Gisin, Electron. Lett. **37**, 26 (2001).
[10]K.-H. Luo, H. Herrmann, S. Krapick, B. Brecht, R. Ricken, V. Quiring, H. Suche, W. Sohler, and C. Silberhorn, New J. Phys. **17**, 073039 (2015).
[11]O. Alibart, V. D'Auria, M. De Micheli, F. Doutre, F. Kaiser, L. Labonté, T. Lunghi, É. Picholle, and S. Tanzilli, J. Opt. **18**, 104001 (2016).
[12]Y. Qi and Y. Li, "Integrated lithium niobate photonics," Nanophotonics **9**, 1287 (2020).
[13]A. Boes, B. Corcoran, L. Chang, J. Bowers, and A. Mitchell, Laser Photonics Rev. **12**, 1700256 (2018).
[14]D. Sun, Y. Zhang, D. Wang, W. Song, X. Liu, J. Pang, D. Geng, Y. Sang, and H. Liu, Light: Sci. Appl. **9**, 197 (2020).
[15]R. A. Becker, Appl. Phys. Lett. **45**, 121 (1984).
[16]Y. Furukawa, K. Kitamura, and G. Foulon, Appl. Phys. Lett. **78**, 1970 (2001).
[17]S. Dezhong and H. Chaoen, Prog. Cryst. Growth Charact. **11**, 269 (1985).
[18]J. D. Bierlein and H. Vanherzeele, J. Opt. Soc. Am. B **6**, 622 (1989).
[19]J. D. Bierlein, A. Ferretti, L. H. Brixner, and W. Y. Hsu, in Optical Fiber Communication Conference, OSA Technical Digest Series, 1987, paper PDP5.
[20]J. D. Bierlein, A. Ferretti, L. H. Brixner, and W. Y. Hsu, Appl. Phys. Lett. **50**, 1216 (1987).
[21]C. Liljestrand, Ph.D. thesis, Laser Physics, Royal Institute of Technology, 2017; ISBN: 978-91-7729-413-9.
[22]C. Canalias and V. Pasiskevicius, Nat. Photonics **1**, 459 (2007).
[23]K.-H. Luo, V. Ansari, M. Massaro, M. Santandrea, C. Eigner, R. Ricken, H. Herrmann, and C. Silberhorn, Opt. Express **28**, 3215 (2020).
[24]P. J. Mosley, J. S. Lundeen, B. J. Smith, P. Wasylczyk, A. B. U'Ren, C. Silberhorn, and I. A. Walmsley, Phys. Rev. Lett. **100**, 133601 (2008).
[25]A. A. Shukhin, D. O. Akatiev, I. Z. Latypov, A. V. Shkalikov, and A. A. Kalachev, J. Phys.: Conf. Ser. **613**, 012015 (2015).
[26]A. Christ, A. Fedrizzi, H. Hübel, T. Jennewein, and C. Silberhorn, in *Single-Photon Generation and Detection: Parametric Down-Conversion*, Experimental Methods in the Physical Sciences (Academic Press, 2013), Chap. 11.
[27]D. B. Ostrowsky and R. Reinisch, *Guided Wave Nonlinear Optics* (Springer Netherlands, 1992).
[28]A. Boudrioua, *Photonic Waveguides: Theory and Applications* (John Wiley & Sons, 2013).
[29]M. N. Armenise, IEE Proc.-J: Optoelectron. **135**, 85 (1988).
[30]D. Eger, M. Oron, and M. Katz, J. Appl. Phys. **74**, 4298 (1993).
[31]M. G. Roelofs, A. Suna, W. Bindloss, and J. D. Bierlein, J. Appl. Phys. **76**, 4999 (1994).
[32]J. Crank, *The Mathematics of Diffusion* (Oxford University Press, 1979).
[33]M. Bazzan and C. Sada, Appl. Phys. Rev. **2**, 040603 (2015).
[34]R. Osellame, M. Lobino, N. Chiodo, M. Marangoni, G. Cerullo, and R. Ramponi, Appl. Phys. Lett. **90**, 241107 (2007).
[35]F. Laurell, T. Calmano, S. Müller, P. Zeil, C. Canalias, and G. Huber, Opt. Express **20**, 22308 (2012).
[36]S. Müller, T. Calmano, P. W. Metz, C. Kränkel, C. Canalias, C. Liljestrand, F. Laurell, and G. Huber, Opt. Lett. **39**, 1274 (2014).
[37]P. D. Townsend, Nucl. Instrum. Methods Phys. Res., Sect. B **46**, 18 (1990).
[38]A. Boudrioua, F. Laurell, P. Moretti, and J. C. Loulergue, J. Opt. Soc. Am. B **18**, 1832 (2001).
[39]J.-J. Yin, F. Lu, X.-B. Ming, Z.-H. Qin, and Y.-J. Ma, Appl. Opt. **51**, 2400 (2012).
[40]L.-L. Wang, K.-M. Wang, F. Lu, B.-R. Shi, X.-L. Wang, L. Wang, and Q.-M. Lu, J. Appl. Phys. **104**, 063115 (2008).
[41]H. Tamada, A. Yamada, and M. Saitoh, J. Appl. Phys. **70**, 2536 (1991).
[42]W. M. Young, M. M. Fejer, M. J. F. Digonnet, A. F. Marshall, and R. S. Feigelson, J. Lightwave Technol. **10**, 1238 (1992).
[43]R. Regener and W. Sohler, J. Opt. Soc. Am. B **5**, 267 (1988).
[44]F. Laurell and G. Arvidsson, J. Opt. Soc. Am. B **5**, 292 (1988).
[45]R. C. Miller and A. Savage, Appl. Phys. Lett. **9**, 169 (1966).
[46]H. Vanherzeele and J. D. Bierlein, Opt. Lett. **17**, 982 (1992).
[47]I. P. Kaminow, V. Ramaswamy, R. V. Schmidt, and E. H. Turner, Appl. Phys. Lett. **24**, 622 (1974).
[48]J. L. Jackel, R. E. Howard, E. L. Hu, and S. P. Lyman, Appl. Phys. Lett. **38**, 907 (1981).
[49]T. Sugita, K. Mizuuchi, K. Yamamoto, K. Fukuda, T. Kai, I. Nakayama, and K. Takahashi, Electron. Lett. **40**, 1359 (2004).
[50]W. J. Park, W. S. Yang, W. K. Kim, H. Y. Lee, J.-W. Lim, M. Isshiki, and D. H. Yoon, Opt. Mater. **28**, 216 (2006).
[51]H. J. Lee and S.-Y. Shin, Electron. Lett. **31**, 268 (1995).
[52]J. M. de Mendívil, J. del Hoyo, J. Solís, and G. Lifante, Opt. Mater. **62**, 353 (2016).
[53]R. Takigawa, K. Kamimura, K. Asami, K. Nakamoto, T. Tomimatsu, and T. Asano, Jpn. J. Appl. Phys., Part 1 **59**, SBBD03 (2020).
[54]T. Kawaguchi, T. Yoshino, J. Kondo, A. Kondo, S. Yamaguchi, and K. Noda, in *Technical Digest. Summaries of Papers Presented at the Conference on Lasers and Electro-Optics. Postconference Technical Digest* (IEEE, 2001), Cat. No. 01CH37170.
[55]J. Sun, Y. Gan, and C. Xu, Opt. Lett. **36**, 549 (2011).
[56]R. V. Schmidt and I. P. Kaminow, Appl. Phys. Lett. **25**, 458 (1974).
[57]K. Sugii, M. Fukuma, and H. Iwasaki, J. Mater. Sci. **13**, 523 (1978).
[58]T. Suhara and M. Fujimura, *Waveguide Nonlinear-Optic Devices* (Springer Berlin Heidelberg, 2003).
[59]M. Fukuma and J. Noda, Appl. Opt. **19**, 591 (1980).
[60]S. Miyazawa, J. Appl. Phys. **50**, 4599 (1979).
[61]S. Thaniyavarn, T. Findakly, D. Booher, and J. Moen, Appl. Phys. Lett. **46**, 933 (1985).
[62]G. Schreiber, H. Suche, Y. L. Lee, W. Grundkötter, V. Quiring, R. Ricken, and W. Sohler, Appl. Phys. B **73**, 501 (2001).
[63]M. M. Fejer, M. J. F. Digonnet, and R. L. Byer, Opt. Lett. **11**, 230 (1986).
[64]C. Langrock, S. Kumar, J. E. McGeehan, A. E. Willner, and M. M. Fejer, J. Lightwave Technol. **24**, 2579 (2006).
[65]B. Jaskorzynska, G. Arvidsson, and F. Laurell, Proc. SPIE **0651**, 221 (1986).
[66]S. Pal, B. K. Das, and W. Sohler, Appl. Phys. B **120**, 737 (2015).
[67]L. Ming, C. B. E. Gawith, K. Gallo, M. V. O'Connor, G. D. Emmerson, and P. G. R. Smith, Opt. Express **13**, 4862 (2005).
[68]L. Arizmendi, Phys. Status Solidi A **201**, 175 (2004).
[69]W. M. Young, R. S. Feigelson, M. M. Fejer, M. J. F. Digonnet, and H. J. Shaw, Opt. Lett. **16**, 995 (1991).
[70]L. G. Carpenter, S. A. Berry, R. H. S. Bannerman, A. C. Gray, and C. B. E. Gawith, Opt. Express **27**, 24538 (2019).
[71]M. L. Bortz and M. M. Fejer, Opt. Lett. **16**, 1844 (1991).
[72]G. R. Paz-Pujalt, D. D. Tuschel, G. Braunstein, T. Blanton, S. T. Lee, and L. M. Salter, J. Appl. Phys. **76**, 3981 (1994).
[73]F. Laurell, M. G. Roelofs, and H. Hsiung, Appl. Phys. Lett. **60**, 301 (1992).
[74]Y. N. Korkishko, V. A. Fedorov, M. P. De Micheli, P. Baldi, K. El Hadi, and A. Leycuras, Appl. Opt. **35**, 7056 (1996).
[75]Y. N. Korkishko and V. A. Fedorov, IEEE J. Sel. Top. Quantum Electron. **2**, 187 (1996).
[76]Y. N. Korkishko, V. A. Fedorov, and F. Laurell, IEEE J. Sel. Top. Quantum Electron. **6**, 132 (2000).
[77]Yu. N. Korkishko and V. A. Fedorov, J. Appl. Phys. **82**, 1010 (1997).
[78]K. El Hadi, M. Sundheimer, P. Aschieri, P. Baldi, M. P. De Micheli, D. B. Ostrowsky, and F. Laurell, JOSA B **14**, 3197 (1997).
[79]M. L. Bortz and M. M. Fejer, Opt. Lett. **17**, 704 (1992).
[80]M. L. Bortz, L. A. Eyres, and M. M. Fejer, Appl. Phys. Lett. **62**, 2012 (1993).
[81]P. G. Suchoski, T. K. Findakly, and F. J. Leonberger, Opt. Lett. **13**, 1050 (1988).
[82]E. Glavas, J. M. Cabrera, and P. D. Townsend, J. Phys. D: Appl. Phys. **22**, 611 (1989).
[83]L. Chanvillard, P. Aschiéri, P. Baldi, D. B. Ostrowsky, and M. de Micheli, Appl. Phys. Lett. **76**, 1089 (2000).
[84]O. Stepanenko, E. Quillier, H. Tronche, P. Baldi, and M. De Micheli, IEEE Photonics Technol. Lett. **26**, 1557 (2014).

[85]D. H. Tsou, M. H. Chou, P. Santhanaraghavan, Y. H. Chen, and Y. C. Huang, Mater. Chem. Phys. **78**, 474 (2003).
[86]A. P. Rambu, A. M. Apetrei, F. Doutre, H. Tronche, V. Tiron, M. De Micheli, and S. Tascu, Photonics Res. **8**, 8 (2020).
[87]M. H. Chou, I. Brener, M. M. Fejer, E. E. Chaban, and S. B. Christman, IEEE Photonics Technol. Lett. **11**, 653 (1999).
[88]M. Neradovskiy, E. Neradovskaia, D. Chezganov, E. Vlasov, V. Y. Shur, H. Tronche, F. Doutre, G. Ayenew, P. Baldi, M. De Micheli, and C. Montes, J. Opt. Soc. Am. B **35**, 331 (2018).
[89]T. Kishimoto and K. Nakamura, Jpn. J. Appl. Phys., Part 1 **51**, 012203 (2011).
[90]See https://www.hcphotonics.com/ppln-chips for commercial waveguides from HCPhotonics; accessed 3 July 2020.
[91]F. Lenzini, S. Kasture, B. Haylock, and M. Lobino, Opt. Express **23**, 1748 (2015).
[92]R. Roussev, A. Sridharan, K. Urbanek, R. Byer, and M. Fejer, in *The 16th Annual Meeting of the IEEE Lasers and Electro-Optics Society* (IEEE, 2003).
[93]K. R. Parameswaran, R. K. Route, J. R. Kurz, R. V. Roussev, M. M. Fejer, and M. Fujimura, Opt. Lett. **27**, 179 (2002).
[94]M. Levy, R. M. Osgood, Jr., R. Liu, L. E. Cross, G. S. Cargill III, A. Kumar, and H. Bakhru, Appl. Phys. Lett. **73**, 2293 (1998).
[95]Y. Nishida, H. Miyazawa, M. Asobe, O. Tadanaga, and H. Suzuki, Electron. Lett. **39**, 609 (2003).
[96]M. Iwai, T. Yoshino, S. Yamaguchi, M. Imaeda, N. Pavel, I. Shoji, and T. Taira, Appl. Phys. Lett. **83**, 3659 (2003).
[97]J. Chen, Y. M. Sua, Z. Ma, C. Tang, Z. Li, and Y. Huang, in *Rochester Conference on Coherence and Quantum Optics (CQO-11), OSA Technical Digest* (Optical Society of America, 2019), paper W6A.18.
[98]I. Krasnokutska, J.-L. J. Tambasco, X. Li, and A. Peruzzo, Opt. Express **26**, 897 (2018).
[99]R. Wolf, I. Breunig, H. Zappe, and K. Buse, Opt. Express **26**, 19815 (2018).
[100]M. Zhang, C. Wang, R. Cheng, A. Shams-Ansari, and M. Lončar, Optica **4**, 1536 (2017).
[101]R. Wu, J. Lin, M. Wang, Z. Fang, W. Chu, J. Zhang, J. Zhou, and Y. Cheng, Opt. Lett. **44**, 4698 (2019).
[102]J. X. Zhou, R. H. Gao, J. T. Lin, M. Wang, W. Chu, W. Li, D. Yin, L. Deng, Z. Fang, J. Zhang, R. Wu, and Y. Cheng, Chin. Phys. Lett. **37**, 084201 (2020).
[103]I. Krasnokutska, R. J. Chapman, J. J. Tambasco, and A. Peruzzo, Opt. Express **27**, 17681 (2019).
[104]N. Yao, J. Zhou, R. Gao, J. Lin, M. Wang, Y. Cheng, W. Fang, and L. Tong, Opt. Express **28**, 12416 (2020).
[105]L. He, M. Zhang, A. Shams-Ansari, R. Zhu, C. Wang, and M. Lončar, Opt. Lett. **44**, 2314 (2019).
[106]C. Wang, C. Langrock, A. Marandi, M. Jankowski, M. Zhang, B. Desiatov, M. M. Fejer, and M. Lončar, Optica **5**, 1438 (2018).
[107]A. Rao, K. Abdelsalam, T. Sjaardema, A. Honardoost, G. F. Camacho-Gonzalez, and S. Fathpour, Opt. Express **27**, 25920 (2019).
[108]S. Kurimura, Y. Kato, M. Maruyama, Y. Usui, and H. Nakajima, Appl. Phys. Lett. **89**, 191123 (2006).
[109]F. Laurell, J. B. Brown, and J. D. Bierlein, Appl. Phys. Lett. **62**, 1872 (1993).
[110]F. Laurell, J. B. Brown, and J. D. Bierlein, Appl. Phys. Lett. **60**, 1064 (1992).
[111]M. G. Roelofs, P. A. Morris, and J. D. Bierlein, J. Appl. Phys. **70**, 720 (1991).
[112]F. Laurell, Opt. Mater. **11**, 235 (1999).
[113]C. J. van der Poel, J. D. Bierlein, J. B. Brown, and S. Colak, Appl. Phys. Lett. **57**, 2074 (1990).
[114]F. Laurell, M. G. Roelofs, W. Bindloss, H. Hsiung, A. Suna, and J. D. Bierlein, J. Appl. Phys. **71**, 4664 (1992).
[115]L. Padberg, M. Santandrea, M. Rüsing, J. Brockmeier, P. Mackwitz, G. Berth, A. Zrenner, C. Eigner, and C. Silberhorn, Opt. Express **28**, 24353 (2020).
[116]P. Mutter, C. C. Kores, M. Widarsson, A. Zukauskas, F. Laurell, and C. Canalias, Opt. Express **28**, 38822 (2020).
[117]F. Laurell, Electron. Lett. **29**, 1629 (1993).
[118]C. Eigner, L. Padberg, M. Santandrea, H. Herrmann, B. Brecht, and C. Silberhorn, Opt. Express **28**, 32925 (2020).
[119]C. Eigner, M. Santandrea, L. Padberg, M. F. Volk, C. E. Rüter, H. Herrmann, D. Kip, and C. Silberhorn, Opt. Express **26**, 28827 (2018).
[120]M. F. Volk, C. E. Rüter, M. Santandrea, C. Eigner, L. Padberg, H. Herrmann, C. Silberhorn, and D. Kip, Opt. Mater. Express **8**, 82 (2018).
[121]C. Chen, C. E. Rüter, M. F. Volk, C. Chen, Z. Shang, Q. Lu, S. Akhmadaliev, S. Zhou, F. Chen, and D. Kip, Opt. Express **24**, 16434 (2016).
[122]C. C. Kores, P. Mutter, H. Kianirad, C. Canalias, and F. Laurell, Opt. Express **26**, 33142 (2018).
[123]V. Boutou, A. Vernay, C. Félix, F. Bassignot, M. Chauvet, D. Lupinski, and B. Boulanger, Opt. Lett. **43**, 3770 (2018).
[124]M. M. Fejer, G. A. Magel, D. H. Jundt, and R. L. Byer, IEEE J. Quantum Electron. **28**, 2631 (1992).